Gallery of Fluid Motion

Eel-like robot swims more efficiently with increasing joint amplitudes compared to constant joint amplitudes

Alexandros Anastasiadis,[1] Annalisa Rossi,[1] Laura Paez,[1] Kamilo Melo,[2] Eric D. Tytell,[3] Auke J. Ijspeert,[1] and Karen Mulleners[1,*]

[1]*Ecole Polytechnique Fédérale de Lausanne (EPFL), Lausanne, Switzerland*
[2]*KM-RoBoTa, Renens, Switzerland*
[3]*Tufts University, Medford, USA*

(Received 10 June 2024; published 22 November 2024)

This paper is associated with a video winner of a 2023 American Physical Society's Division of Fluid Dynamics (DFD) Gallery of Fluid Motion Award for work presented at the DFD Gallery of Fluid Motion. The original video is available online at the Gallery of Fluid Motion, https://doi.org/10.1103/APS.DFD.2023.GFM.V0048 marker GFM.

DOI: 10.1103/PhysRevFluids.9.110509

Eels swim by undulating their body, introducing a traveling wave that propagates from the head to the tail [1]. They can swim for thousands of kilometres without feeding, demonstrating high hydrodynamic efficiency for their traveling wave kinematics [2]. The traveling wave of eels and a wide variety of fish gradually increases in lateral amplitude from the head to the tail [3]. For simulated swimmers, the increasing amplitude envelope shows energetic benefits reducing the swimming cost [4–6]. In our Gallery of Fluid Motion video, we introduced our bio-inspired eel-like robot 1-guilla [Fig. 1(a)], and presented the tradeoff between speed and efficiency in undulatory swimming for a constant joint amplitude traveling wave input [7]. Here, we present how the swimming performance changes when our robot has a joint amplitude that increases along its body, similar to that of fishes.

The robot 1-guilla consists of a computational segment with the battery and wireless communication, a chain of eight motors, and a flexible tail, with a total body length of $L = 0.85\,\mathrm{m}$. The robot swims on the surface of the water, using open loop control, along the length of a swimming pool ($6 \times 2 \times 0.3\,\mathrm{m}$) at EPFL. A camera (GoPro Hero 9, $1920 \times 1080\,\mathrm{px}$) placed atop the pool records movies of the freely swimming robot in the pool under ambient light with a spatial resolution of $552\,\mathrm{px/m}$ and an acquisition rate of 30 Hz. From the individual movie frames, we extract the midline of the undulating robot [Fig. 1(b)] and fit a second-degree polynomial to all points of all recorded midlines for five periods of motion to obtain the global trajectory of the robot and its average swimming speed ($\overline{U}$). The prescribed joint kinematics for the motor joints are a traveling wave characterized by the input joint amplitude (A_{joint}), spatial wavelength (λ_{input}), and frequency (f). The evolution of the midlines projected on the main direction of swimming for one undulation period are shown in Figs. 1(c) and 1(d) for input swimming kinematics with an increasing and constant joint amplitude, respectively. For the constant joint amplitude kinematics

*Contact author: karen.mulleners@epfl.ch

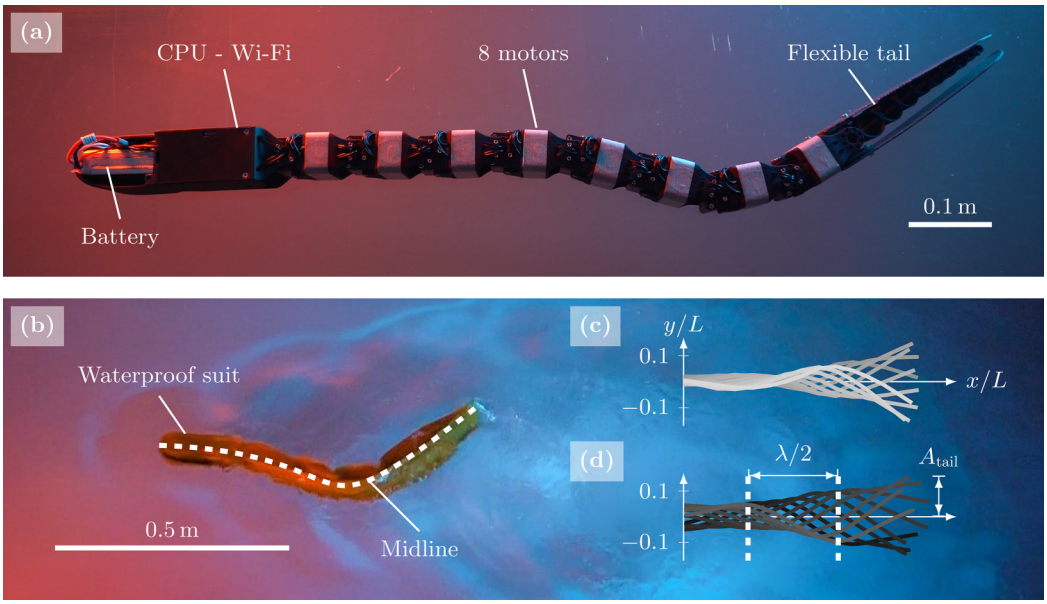

FIG. 1. Overview of the experimental setup using snapshots from the video. (a) Bio-inspired robot 1-guilla. (b) 1-guilla during swimming in its waterproof suit. An example of the midline is plotted on top of the robot. (c) Example midlines projected on the main direction of motion for increasing joint amplitude input for $\lambda_{\text{input}} = 0.64$ and $A_{\text{joint,max}} = 30\,^{\circ}$. (d) Example midlines for constant joint amplitude input for $\lambda_{\text{input}} = 0.71$ and $A_{\text{joint,max}} = 25\,^{\circ}$. The wavelength ($\lambda$) is evaluated as twice the average projected distance between local peaks in curvature. The tail amplitude (A_{tail}) is calculated as half the peak-to-peak distance of the tip of the flexible tail normal to the swimming direction.

[Fig. 1(d)], the joint amplitude has a constant maximum value along the body: $A_{\text{joint}} = A_{\text{joint,max}}$. For the increasing joint amplitude kinematics [Fig. 1(c)] the increase is defined by a polynomial derived from observations of American eels [8]: $A_{\text{joint}}(s_{\text{i}}) = (1 + 0.323(s_{\text{i}} - 1) + 0.310(s_{\text{i}}^2 - 1))A_{\text{joint,max}}$, where s_{i} is the length-normalized position of the ith motor joint. The midline projection enables us to evaluate the tail amplitude (A_{tail}) and the performed wavelength (λ). The average power consumption $\overline{P}$ of the motors of the robot is also recorded for each measurement. More details on the experimental procedure are described in [7].

Experiments are conducted for a range of maximum joint amplitudes $A_{\text{joint,max}}$ and wavelengths λ_{input}, and their swimming performance is evaluated by their speed and efficiency. The speed is presented in terms of the normalized stride length ($\overline{U}/fL$). Efficiency is presented as a dimensional cost of transport ($CoT = \overline{P}/\overline{U}$ with units J/m). Performance metrics are presented as contour plots [Figs. 2(a)–2(d)].

For kinematics with constant joint amplitudes, the robot achieves maximum speed for normalized wavelengths λ_{input}/L between 0.78 and 0.92, and amplitudes $A_{\text{joint,max}}$ between 23° and 33° [Fig. 2(a)]. The considerable variation in speed with increasing λ_{input} and $A_{\text{joint,max}}$ is illustrated by selected examples in our video. The region of minimal cost of transport is found at lower input wavelengths ($\lambda_{\text{input}}/L = 0.55$ to 0.71) and moderately lower joint amplitudes ($A_{\text{joint,max}} = 13\,^{\circ}$ to $33\,^{\circ}$) [Fig. 2(b)].

For kinematics with increasing joint amplitudes along the body, the robot achieves maximum speed for λ_{input}/L between 0.81 and 1, and maximum input joint amplitude $A_{\text{joint,max}}$ between 32° and 45° [Fig. 2(c)]. The region of minimal cost of transport is found at lower input wavelengths (λ_{input}/L between 0.55 and 0.71) and similar maximum joint amplitudes ($A_{\text{joint,max}}$ between 26° and 42°) [Fig. 2(d)].

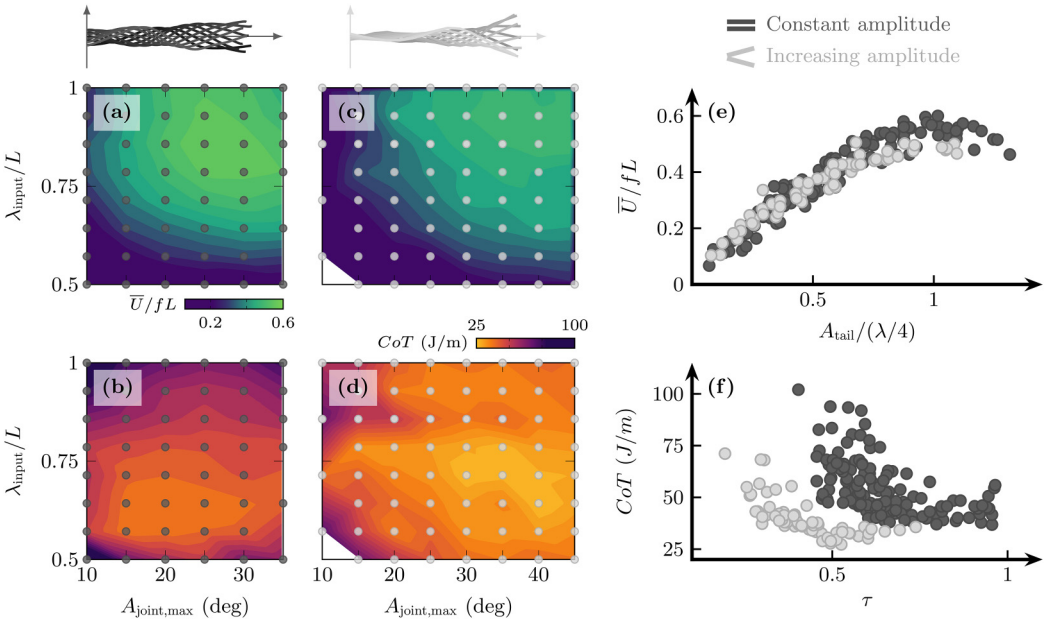

FIG. 2. Performance comparison for constant joint amplitude (dark gray) and increasing joint amplitude (light gray) kinematics. (a), (b) Performance maps of normalized stride length and cost of transport for constant joint amplitude and frequency $f = 1.5$ Hz. (c), (d) Performance maps of normalized stride length and cost of transport for increasing joint amplitude and frequency $f = 1.5$ Hz. (e) Normalized stride length as a function of the specific tail amplitude for kinematics with constant (dark gray) and increasing (light gray) joint amplitudes. (f) Cost of transport as a function of the traveling wave index for kinematics with constant (dark gray) and increasing (light gray) joint amplitudes.

The optimal stride length region is larger for constant joint amplitude kinematics [Fig. 2(a)] than for increasing joint amplitude kinematics [Fig. 2(c)]. The maximum stride length is slightly lower for the kinematics with an increasing joint amplitude, but their cost of transport is overall lower than for the constant joint amplitude kinematics. The region of low cost of transport is significantly larger in Fig. 2(d) compared to Fig. 2(b). Overall, optimum regions within the range of kinematics tested are present for both stride length and cost of transport performance maps for both types of kinematics.

The stride length is mainly characterized by the specific tail amplitude [$A_{tail}/(\lambda/4)$] for both types of kinematics tested here [Fig. 2(e)]. The input joint amplitude, examined above, does not directly determine the tail beat amplitude, because of motion and rotation about the center of mass. When the specific tail amplitude increases, the stride length increases until reaching a maximum value at the specific tail amplitude of unity [7]. Further increase of the specific tail amplitude is accompanied by a decrease in stride length. For the constant joint amplitude kinematics, the maximum normalized stride length achieved was $(\overline{U}/fL)_{max,const} = 0.6$. For the increasing joint amplitude kinematics, the maximum value was $(\overline{U}/fL)_{max,\nearrow} = 0.5$. Overall, the tail governs the stride length, but for kinematics with constant joint amplitudes, the maximum stride length achieved is higher, possibly because the body's anterior part has higher amplitudes.

The cost of transport is characterized by the traveling wave index (τ) [Fig. 2(f)]. The traveling wave index quantifies the resemblance of a waveform to a pure traveling wave ($\tau = 1$) [9]. For increasing traveling wave indices, the cost of transport decreases [7,10]. This trend is observed for both types of kinematics tested here. For the constant joint amplitude kinematics, the minimum cost of transport was $CoT_{min,const} = 36.8$ J/m. For the increasing joint amplitude kinematics, the

minimum value was $CoT_{\min,\nearrow} = 28.2\,\mathrm{J/m}$. Lower cost of energy swimming is achieved for a traveling wave motion with decreased lateral displacement of the anterior part of the body.

Overall, the increasing joint amplitude kinematics reduce the maximum achievable stride length but also reduce the energetic costs of swimming for our bio-inspired undulatory robot, suggesting that animals might have similar energetic benefits when they are observed to swim with such an amplitude profile. For an increasing joint amplitude, the maximum achievable stride length is reduced by 12% across the range of tested kinematics compared to their constant joint amplitude counterparts. The stride-length reduction suggests that for an undulatory swimming robot, and potentially for an animal, it is worth switching to constant joint amplitude kinematics to swim faster at the same frequency. For an increasing joint amplitude, the minimum cost of transport is reduced by 22% compared to their constant joint amplitude counterparts. To the extent that the hydrodynamic forces govern the swimmers' energy expenditure, we expect a similar trend for animal swimming, which may explain the observed kinematics of fish. Of course, the energetic needs of the muscles of live animals differ significantly from the needs of the electric motors of our robot. For bio-inspired undulatory robots, we provide evidence that using a bio-inspired increasing amplitude can be crucial to reduce the swimming cost of transport and increase the traveling range of the robot. In addition to acting as the star of our video, our robot can provide insights for animal observations and further development of bio-inspired robots.

ACKNOWLEDGMENTS

This work was financially supported by the STI eSeed programme at EPFL. A.R. was supported by the EPFL Excellence in Engineering (E3) programme. E.D.T. was supported by a Swiss National Science Foundation scientific exchange grant (IZSEZ0_194755) and by the U.S. National Science Foundation (NSF IOS 1652582).

[1] R. E. Shadwick and G. V. Lauder (eds.), *Fish Physiology: Fish Biomechanics* (Academic Press, San Diego, CA, 2006).

[2] V. van Ginneken and G. E. E. J. M. van den Thillart, Physiology: Eel fat stores are enough to reach the Sargasso, Nature (London) **403**, 156 (2000).

[3] V. D. Santo, E. Goerig, D. K. Wainwright, O. Akanyeti, J. C. Liao, T. Castro-Santos, and G. V. Lauder, Convergence of undulatory swimming kinematics across a diversity of fishes, Proc. Natl. Acad. Sci. USA **118**, e2113206118 (2021).

[4] A. Maertens, A. Gao, and M. S. Triantafyllou, Optimal undulatory swimming for a single fish-like body and for a pair of interacting swimmers, J. Fluid Mech. **813**, 301 (2017).

[5] N. Nangia, R. Bale, N. Chen, Y. Hanna, and N. A. Patankar, Optimal specific wavelength for maximum thrust production in undulatory propulsion, PLoS ONE **12**, e0179727 (2017).

[6] S. Kern and P. Koumoutsakos, Simulations of optimized anguilliform swimming, J. Exp. Biol. **209**, 4841 (2006).

[7] A. Anastasiadis, L. Paez, E. Tytell, A. J. Ijspeert, and K. Mulleners, Identification of the trade-off between speed and efficiency in undulatory swimming using a bio-inspired robot, Sci. Rep. **13**, 15032 (2023).

[8] E. D. Tytell and G. V. Lauder, The hydrodynamics of eel swimming: I. Wake structure, J. Exp. Biol. **207**, 1825 (2004).

[9] B. F. Feeny, A complex orthogonal decomposition for wave motion analysis, J. Sound Vib. **310**, 77 (2008).

[10] P. Leroy-Calatayud, M. Pezzulla, A. Keiser, K. Mulleners, and P. M. Reis, Tapered foils favor traveling-wave kinematics to enhance the performance of flapping propulsion, Phys. Rev. Fluids **7**, 074403 (2022).